1 # PV-specific loss of the transcriptional coactivator PGC-1α slows down the
2 # evolution of epileptic activity in an acute ictogenic model.

3 **Authors:** R. Ryley Parrish[1†], Connie Mackenzie-Gray-Scott[1†], Darren Walsh[1], Claudia Racca[1],

4 Rita M. Cowell[2] and Andrew J. Trevelyan[1*]

5

6 [1]Newcastle University Biosciences Institute, Medical School, Framlington Place, Newcastle

7 upon Tyne, NE2 4HH, UK.

8 [2] Department of Neuroscience, Drug Discovery Division at Southern Research, Birmingham,

9 AL 35205, USA; Department of Cell, Developmental and Integrative Biology, University of

10 Alabama at Birmingham, Birmingham, AL 35294, USA.

11

12 † Equal contribution.

13 *Correspondence to: andrew.trevelyan@ncl.ac.uk

14

15 **Abbreviated title**: Loss of cortical PGC-1α slows down ictogenesis

16 The authors declare no conflicts of interest

17 **Number of pages:**   **16**

18 **Number of figures:** **8**

19 **Word counts**

20 **Abstract:**   **247 (250 max)**

21 **Introduction:**   **580 (650 max)**

22 **Discussion:**   **764 (1500 max)**

Abstract

26

27   The transcriptional coactivator, PGC-1α (peroxisome proliferator activated receptor
28 gamma coactivator 1α), plays a key role coordinating energy requirement within cells.
29 Its importance is reflected in the growing number of psychiatric and neurological
30 conditions that have been associated with reduced PGC-1α levels. In cortical networks,
31 PGC-1α is required for the induction of parvalbumin (PV) expression in interneurons,
32 and PGC-1α deficiency affects synchronous GABAergic release. It is unknown, however,
33 how this affects cortical excitability. We show here that knocking down PGC-1α
34 specifically in the PV-expressing cells (PGC-1α$^{PV-/-}$), blocks the activity-dependent
35 regulation of the synaptic proteins, *SYT2* and *CPLX1*. More surprisingly, this cell-class
36 specific knock-out of PGC-1α appears to have a novel anti-epileptic effect, as assayed in
37 brain slices bathed in 0 Mg^{2+} media. The rate of pre-ictal discharges developed
38 approximately equivalently in wild-type and PGC-1α$^{PV-/-}$ brain slices, but the intensity of
39 these discharges was lower in PGC-1α$^{PV-/-}$ slices, as evident from the reduced power in
40 the gamma range and reduced firing rates in both PV interneurons and pyramidal cells
41 during these discharges. Reflecting this reduced intensity in the pre-ictal discharges, the
42 PGC-1α$^{PV-/-}$ brain slices experienced many more discharges before transitioning into a
43 seizure-like event. Consequently, there was a large increase in the latency to the first
44 seizure-like event in brain slices lacking PGC-1α in PV interneurons. We conclude that
45 knocking down PGC-1α limits the range of PV interneuron firing, and this slows the
46 pathophysiological escalation during ictogenesis.

47

Introduction

49   Studies in non-neuronal tissue have identified the transcriptional coactivator, PGC-1α
50 (peroxisome proliferator activated receptor gamma coactivator 1α), as a key regulator of
51 expression of nuclear encoded mitochondrial genes (Austin and St-Pierre, 2012; Handschin
52 and Spiegelman, 2006; Lin et al., 2005; McMeekin et al., 2021). Its expression is induced by
53 various triggers, including exercise, cold and fasting, and it then drives mitochondrial
54 (Puigserver et al., 2001) and peroxisome biogenesis (Bagattin et al., 2010) and uncouples
55 mitochondrial respiration (St-Pierre et al., 2003). PGC-1α is also highly expressed in different
56 parts of the brain, where its expression is enriched in GABAergic neurons (Cowell et al., 2007).
57 Within cortical networks, PGC-1α appears particularly to affect parvalbumin-expressing (PV)

2

58   interneurons (Cowell et al., 2007): the highest transcriptomic counts of PGC-1α are found in
59   this subset of cortical neurons (Saunders et al., 2018); reduced PGC-1α expression
60   (heterozygotes and homozygote knock-out) leads to a loss of PV in a dose-dependent manner,
61   without affecting the expression of other interneuronal markers, while overexpression of PGC-
62   1α in cultured neurons strongly induces PV expression (Lucas et al., 2010). Consistent with
63   these findings, PV interneurons ordinarily have a very high mitochondrial content, and express
64   cytochrome c more intensely than other cortical neurons (Gulyas et al., 2006; Kageyama and
65   Wong-Riley, 1982). PV interneurons are also among the most active of any cortical neuronal
66   class; they characteristically fire on every cycle of gamma oscillations (Atallah and Scanziani,
67   2009; Hajos et al., 2004; Whittington and Traub, 2003) and show extremely high firing rates
68   ahead of an ictal wavefront (Parrish et al., 2019; Sessolo et al., 2015). These various
69   considerations – their apparent high metabolism, and the powerful effect that PV interneurons
70   exert upon cortical networks – have led to the suggestion that PV interneurons may be
71   particularly susceptible to metabolic stress, which in turn could give rise to neuropathology
72   (Kann, 2016; Whittaker et al., 2011). It is relevant, therefore, that reduced PGC-1α expression
73   has been found in a number of neurological conditions (McMeekin et al., 2021), including
74   Parkinson's disease (Zheng et al., 2010), Alzheimer's disease (Qin et al., 2009; Sheng et al.,
75   2012), Huntington's disease (Cui et al., 2006), multiple sclerosis (Witte et al., 2013), and
76   schizophrenia (Christoforou et al., 2007; Jiang et al., 2013a), but interestingly, not epilepsy.
77   Germline knockdown of PGC-1α is associated with hyperactive behaviour (Lin et al., 2004),
78   although this is believed to be a behavioural adaptation to a reduction in thermogenesis capacity
79   in brown fat and muscle, because the hyperactive phenotype was not replicated in mice with
80   central nervous system deletion of PGC-1α (Lucas et al., 2012).

81   Knocking-out PGC-1α selectively in PV interneurons (PGC-1α$^{PV-/-}$) also affects synaptic
82   function, with a marked drop in two synaptic proteins, synaptotagmin 2 (Syt2) and complexin
83   1 (Cplx1), a reduction in synchronous GABA release, and impaired long-term memory (Lucas
84   et al., 2014). Intriguingly, the effects on GABAergic synaptic function were somewhat
85   inconsistent in hippocampal and neocortical networks (Dougherty et al., 2014; Lucas et al.,
86   2014; Lucas et al., 2010). These changes might be expected to alter network excitability, so we
87   investigated how epileptiform activity develops in brain slices prepared from these mice,
88   compared to age-matched wild-type controls, when bathed in artificial cerebro-spinal fluid
89   (aCSF) lacking Mg^{2+} ions ($0Mg^{2+}$ model). Both experimental groups showed preictal activity
90   occurring at similar rates, but the intensity of these discharges, as measured by the gamma

3

91   bandwidth power, and the mean firing rates in both PV and pyramidal neurons, was lower in

92   the brain slices prepared from PGC-1α$^{PV-/-}$ mice. Perhaps reflecting this lower intensity of

93   discharge, the knock-out brain slices experienced many more preictal events prior to the first

94   seizure-like event (SLE), and consequently, also showed a significantly longer latency until

95   this first SLE. Altogether, these data indicate that lack of PGC-1α within inhibitory PV cells

96   acts as a restraint on runaway excitation within cortical networks, having a neuroprotective

97   effect during induced epileptogenesis. This result demonstrates a role for PGC-1α in

98   influencing cortical excitability through transcriptional regulation of PV cell activity.

99

Methods

101   **Animals**: All procedures were performed according to the guidelines of the Home Office UK

102   and animals (Scientific Procedures) Act 1986. All the data were collected from adult male and

103   female mice (2 – 6 months). Wild type (C57/BL6) mice or PVCreHet mice (Stock # 008069,

104   The Jackson Laboratory, Bar Harbor, ME USA) were used as control animals for all

105   experiments. No difference was observed in the 0 Mg^{2+} induced activity between wild type

106   and PVCreHet mice, so these groups were combined and labelled "WT" in the study.

107   Conditional deletion of PGC-1α within PV interneurons was achieved by crossing mice with

108   LoxP sites flanking the exon 3–5 region of the PGC-1α gene (PGC-1α$^{fl/fl}$, Stock # 009666, The

109   Jackson Laboratory) with mice expressing Cre recombinase driven by PV (mentioned above)

110   on a C57BL/6 background on which they were maintained. Briefly, a line of homozygous PGC-

111   1α$^{fl/fl}$ mice were created and crossed with a homozygous PVCre mouse line to generate the

112   experimental animals with the genotype PVCre:PGC-1α$^{fl/+}$. All animals were group housed in

113   individually ventilated cages kept at room temperature with a 12hour/12hour light/dark cycle

114   and provided with food and water *ad libitum.*

115   **Viral injections:** To allow visualization of PV interneurons for the patch clamp experiments,

116   2-4 month old PVCre or PGC-1α.PVCre animals were injected with AAV9.Floxxed.MCherry

117   viral vector (Penn Vector Core, University of Pennsylvania). Mice were anaesthetised by

118   intraperitoneal injection of ketamine (75 mg kg^{-1}, Ketalar™ Injection, Pfizer Ltd., Sandwich,

119   UK) combined with medetomidine (1 mg kg^{-1}, Domitor®, Janssen Animal Health,

120   Basingstoke, UK) and were then transferred to a stereotaxic frame where anaesthesia was

121   maintained using inhalational administration of isofluorane (3-5% for induction and 2% for

122   maintenance, delivered in 0$_2$ at 400-800ml/min). The head was shaved and disinfected with

4

123 chlorhexidine. A craniotomy was performed to reveal the dorsal right cortex, and two
124 injections were made of the viral vector (1 in 10 dilution) separated along the antero-posterior
125 axis (~1mm and 2mm posterior to bregma) and at the same mediolateral location (~1.5-2mm
126 lateral to the midline). The viral vector was delivered by pressure injection (Ultramicropump
127 3, World Precision Instruments), through a 10μl Hamilton syringe, with a bevelled 36 gauge
128 needle (World Precision Instruments). At each site, a total of 1μl was injected at a rate of 5-
129 10nl/s, at 3 depths (200 / 400 / 400nl at 1 / 0.7 / 0.4mm, respectively, deep to the pia). The
130 needle was left *in situ* for 3 mins after the final injection, to prevent back-tracking of the
131 injected particles out of the injection track. Post-operatively, mice were given subcutaneous
132 injection of atipamezole (5 mg kg^{-1}, Janssen Animal Health) and meloxicam (5 mg kg^{-1}) to
133 reverse the anaesthesia and provide post-operative pain relief. The animals were allowed to
134 recover in a heated and ventilated incubation chamber overnight and monitored at 2 and 24
135 hours post-surgery. Some animals were given further doses of meloxicam and fluids, as
136 required, based upon clinical assessment of their post-operative recovery, using body weight
137 and behavioural scoring. Animals were subsequently assessed for their general health twice a
138 day, for 5 days, and then weekly for 2-5 more weeks, prior to being sacrificed to prepare brain
139 slices.

140 **Brain slice preparation:** Mice were sacrificed by cervical dislocation followed by immediate
141 decapitation. The brain was removed and sliced into ice-cold cutting solution containing (in
142 mM): (3 MgCl$_2$; 126 NaCl; 2.6 NaHCO$_3$; 3.5 KCl; 1.26 NaH$_2$PO$_4$; 10 glucose), using a Leica
143 VT1200 vibratome (Nussloch, Germany). We used 400μm horizontal sections, containing
144 entorhinal cortex (EC) and neocortex, for local field potential (LFP) recordings, and 350μm
145 coronal sections for the patch clamp recordings. Slices were then transferred to an interface
146 tissue holding chamber and incubated for 1 - 2 hours at room temperature in aCSF containing
147 (in mM): (2 CaCl$_2$; 1 MgCl$_2$; 126 NaCl; 2.6 NaHCO$_3$; 3.5 KCl; 1.26 NaH$_2$PO$_4$; 10 glucose).
148 All the solutions were being bubbled continuously to saturate with carboxygen (95% O$_2$ and
149 5% CO$_2$).

150 **Extracellular LFP recordings**: These experiments were performed using interface recording
151 chambers. Slices were placed in the recording chamber perfused with aCSF or aCSF without
152 Mg^{2+}. Recordings were obtained using normal aCSF-filled 1-3MΩ borosilicate glass
153 microelectrodes (GC120TF-10; Harvard apparatus, Kent) placed in deep layers of the
154 neocortex. Microelectrodes were pulled using Narishige electrode puller (Narishige Scientific
155 Instruments, Tokyo, Japan). The temperature of the chamber and perfusate was maintained at

5

156   33-36 °C using a closed circulating heater (FH16D, Grant instruments, Cambridge, UK). The

157   solutions were perfused at the rate of 3-4mls/min by a peristaltic pump Watson Marlow 501U

158   (Watson-Marlow Pumps Limited, Cornwall UK). Waveform signals were acquired using

159   BMA-931 biopotential amplifier (Dataq instruments, Akron, USA), Micro 1401-3 ADC board

160   (Cambridge Electronic Design, UK) and Spike2 version 7.10 software (Cambridge Electronic

161   Design, UK). Signals were sampled at 10 kHz, amplified (gain: 500) and bandpass filtered (1-

162   3000Hz). CED4001-16 Mains Pulser (Cambridge Electronic Design, UK) was connected to

163   the events input of CED micro 1401-3 ADC board and was used to remove 50Hz hum offline.

164   Extracellular field recordings were analysed to detect pathological discharges using a custom-

165   written code in Matlab2018b (Mathworks, MA, USA) which can be provided upon request. In

166   brief, this used a frequency-domain analysis to detect periods when the LFP power exceeded

167   baseline activity by a designated threshold. Using the spectrogram.m macro, in Matlab (bin

168   width 0.128s, with 50% time shifts), we derived the mean and standard deviation for an epoch

169   of baseline lasting at least 10s, for frequencies between 1-150Hz (50 subdivisions, on a log

170   scale). The spectrogram was then performed for the entire recording, and normalized to the

171   baseline mean and standard deviation for each frequency bandwidth individually. To avoid

172   contamination with mains noise, we omitted frequencies between 48-52Hz. This process

173   generated a z-score spectrogram, in which the pixels represented the excess power at a

174   particular frequency, for a specific time bin (0.128s), in terms of standard deviations from the

175   baseline mean. Using a threshold of 3 standard deviations above the baseline mean, we

176   identified all time bins for which any frequency exceeded this threshold. These were summed

177   cumulatively, to estimate the rate and acceleration of pathological activity within the brain

178   slice. Continuous epochs of suprathreshold bins were designated to be single "events", which

179   were then analysed for their total power within the conventional LFP frequency bins (α, γ bands

180   etc) over the whole event.

181   **Patch-clamp recordings**: These recordings were performed in submerged recording

182   chambers. Slices were perfused with aCSF with the same composition as mentioned above at

183   3–5 mL/min and heated to 33–34°C. Whole cell and cell attached data were acquired using

184   pClamp software, Multiclamp 700B, and Digidata acquisition board (Molecular Devices,

185   Sunnyvale, CA, USA). Recording chamber, heater plate (Warner Instruments, Hamden, CT)

186   and micromanipulators (Scientifica,, UK) were mounted on a Scientifica movable top plate

187   fitted to a laser spinning disc-confocal microscope (Visitech, UK). Whole cell and cell attached

188   recordings of layer five neurons within neocortex were made using 4–7 MΩ pipettes (GC150F-

189   10, Harvard apparatus, Kent) pulled using micropipette puller (Model-P87, Sutter Instruments,

190   CA, USA). Pipettes were filled with solution containing (mM): 125 K-gluconate, 6 NaCl, 10

191   HEPES, 2.5 Mg-ATP, 0.3 Na_2-GTP; pH and osmolarity of the electrode-filling solution used

192   was adjusted to 7.4 and 280-285 mOsms, respectively.

193   To investigate the firing properties of pyramidal cells and PV interneurons during induced

194   epileptogenesis dual recordings were made in neocortical layer 5 cells in voltage clamp

195   configuration. First a pyramidal cell was patched in whole cell mode and held at -70mV to act

196   as a reference for the development of ictal-like events in the slice and secondly either a

197   pyramidal or PV cell was patched in cell attached mode to identify spikes during evolving

198   epileptiform activity as monitored by the whole cell reference recording. Once the whole cell

199   and cell attached patch recordings were established, the Mg^{2+} ions were washed out of the

200   bathing aCSF to induce the development of epileptiform activity. For the targeted cell attached

201   patch recordings of PV interneurons the cells were visualised using a spinning disc confocal

202   microscope (UMPlanFL N ×20, 0.5 NA objective) with a rhodamine (U-MRFPHQ) filter set.

203   The tissue was illuminated with a 561 nm laser (Cobolt Jive 50; Cobolt) to visualize the

204   MCherry fluorescence within the PV interneurons of the injected PVCre and PGC-1α.PVCre

205   animals. Hamamatsu C9100 EM cameras (Hamamatsu Photonics (UK), Welwyn Garden City,

206   UK) were used to visualize and capture images, run by Simple PCI software (Digital Pixel,

207   Brighton, UK; microscope 1) installed on a Dell Precision computer (Dell Technologies,

208   Round Rock, TX, USA). Patch clamp data were analysed using custom-written codes in

209   Matlab2018b.

210   **Tissue collection**: After 1 hour of recordings using the interface chamber, tissue was immersed

211   in Ambion RNAlater solution (Thermo Fisher Scientific) and the neocortical tissue was

212   collected. Tissue was then stored in RNAlater solution, at 4 °C until the RNA was extracted

213   **RNA Preparations**: RNA was extracted using the RNAqueous-Micro Total RNA Isolation

214   Kit (Thermo Fisher Scientific) and eluted in 15 µl of provided elution buffer. Residual genomic

215   DNA was removed using reagents supplied in the above kit and done according to the

216   Manufacturer's instructions. Concentration and purity of RNA were determined using a

217   BioDrop DUO (BioDrop, Cambridge, UK). RNA was then stored at -80 °C until the cDNA

218   library preparation.

219   **Real time (RT) PCR**: Samples were normalized to 100 ng prior to the cDNA library

220   preparation. cDNA synthesis was preformed using the Applied Biosystems High-Capacity

221 cDNA Reverse Transcription Kit (Thermo Fisher Scientific) in a Thermo Hybaid PCR Express

222 Thermal Cycler (Thermo Hybaid, Ashford, UK) at a total volume of 20 µl. The cDNA was

223 then diluted 1:4 with nuclease free H_2O. The following primers were used for the RT-PCR:

224 Parvalbumin (For: attgaggaggatgagctggg, Rev: cgagaaggactgagatgggg), c-fos (For:

225 cagcctttcctactaccattcc, Rev: acagatctgcgcaaaagtcc), Glyceraldehyde 3-phosphate

226 dehydrogenase (Gapdh) (For: acctttgatgctggggctggc, Rev: gggctgagttgggatggggact). Ppargc1α

227 (For: agcctctttgcccagatctt, Rev: ggcaatccgtcttcatccac), Syt2 (For: caactcccattcctgaccct, Rev:

228 ttttctccaccgcccatttg), Cplx1 (For: tcagacacacttggagtccc , Rev: cacttgattatgcggccctc). Q-PCR

229 amplifications were performed on a Applied Biosystems Step One Plus RT PCR system

230 (Thermo Fisher Scientific) at 95 °C for 10min, 40 repeats of 95 °C for 10s, followed by 58 °C

231 for 30s, 95 °C for 15s. This protocol was immediately followed by the melt curve starting at

232 95 °C for 15s, 60 °C for 1min, 95 °C for 15s, and, finally, held at 4 °C. All samples were run

233 in duplicate at a primer molarity of 10 µmol/L, and PV, c-fos, Ppargc1α, Syt2, Cplx1 were

234 compared to GAPDH. Expression of GAPDH was unchanged across all treatment groups.

235 Cycle threshold (Ct) values were analysed using the comparative Ct method to calculate

236 differences in gene expression between samples. Samples were run on a DNA agarose gel to

237 confirm expected product size.

238 **Statistical analysis**: Relative mRNA fold changes were analysed using the comparative Ct

239 method. Due to a lack of homogeneity between groups (Brown–Forsythe test and Bartlett's

240 test), mRNA expression data were first transformed using a square root transformation. Square

241 root transformation of mRNA data resulted in a nonsignificant Brown–Forsythe test and

242 Bartlett's test. Transformed data were then analysed using a one-way analysis of variance

243 (ANOVA), with a Tukey post-hoc test for all mRNA expression data of 3 or more groups.

244 Electrophysiology event detection data and mRNA of only two groups were analysed using the

245 student's t-test. Significance was set at $P \leq 0.05$ for all analyses and data represented as mean

246 ± SEM unless stated otherwise. Figures of mRNA expression and event detection, along with

247 all statistics were done using GraphPad Prism (GraphPad Software, Inc., La Jolla, California,

248 USA). Figures of electrophysiology traces were created using Matlab R2018b (MathWorks,

249 USA), Inkscape and Adobe Photoshop.

250

251

8

Results

252

253 Seizure activity rapidly induces a strong expression of proto-oncogenes, including c-fos.

254 This has been demonstrated in a range of *in vivo* models of ictogenesis (Dragunow and

255 Robertson, 1987; Morgan et al., 1987; White and Gall, 1987). Similarly, in brain slices,

256 following an hour of exposure to 0 Mg^{2+} aCSF, c-fos and PGC-1α are strongly up-regulated,

257 as are the synaptic proteins, synaptotagmin 2 (*Syt2*) and complexin 1 (*Cplx1*), while *Pvalb* is

258 significantly down-regulated (Figure 1A). The relevance of these changes in *Syt2*, *Cplx1* and

259 *Pvalb* is that expression of all three have previously been shown to be influenced by PGC-1α

260 levels (Lucas et al., 2014; Lucas et al., 2010). In PGC-1α$^{PV-/-}$ brain slices, *Pvalb*, *Syt2* and

261 *Cplx1* all show greatly reduced expression in the naïve slices (pre-exposure to 0Mg^{2+} aCSF)

262 compared to wild-type slices, and critically, showed no alteration of expression following

263 exposure to 0 Mg^{2+} aCSF (Figure 1B-D), indicating that the activity-induced changes in these

264 genes in wild-type slices are indeed downstream of PGC-1α.

265 The lack of change in gene expression in PGC-1α$^{PV-/-}$ brain slices was not due to a lack of

266 epileptiform activity during the hour exposure to 0Mg^{2+} aCSF; indeed, both sets of brain slices

267 showed the distinctive pattern of evolving pathological discharges (Figure 2A), starting with

268 transient discharges lasting a few hundred milliseconds, and at longer latency, the appearance

269 of sustained rhythmic discharges lasting tens of seconds, which we term seizure-like events

270 (SLEs). The cumulative activity patterns, however, were strikingly different for the two

271 experimental groups (Figure 2B-E). PGC-1α$^{PV-/-}$ brain slices experienced a significantly larger

272 number of preictal events prior to the first SLE (Figure 2B) relative to control brain slices,

273 which cumulatively, represented a much longer duration of pathological activity (Figure 2C).

274 The first SLE happened significantly later in PGC-1α$^{PV-/-}$ brain slices (Figure 2D), while the

275 total number of SLEs within the first 30mins exposure to 0Mg^{2+} aCSF was significantly less,

276 compared to wild-type slices (Figure 2E). The cumulative duration of pathological activity

277 rose steadily in both experimental groups, but because there were so many more preictal events

278 in PGC-1α$^{PV-/-}$ brain slices, the cumulative total in that experimental group achieved a far

279 higher level prior to the first SLE (Figure 3A). Notably, however, the discharge durations

280 remained stable in both groups (Figure 3B; note the constant gradients), and furthermore, there

281 was no difference in gradient between the groups.

282 We next analysed the power spectra of each preictal discharge (Figure 4), which showed

283 that although the durations remain stable, the power across all bandwidths increased

284 progressively, leading up to the first SLE. The low frequency component of the LFP is thought

9

285   to reflect the local synaptic currents, while the high gamma activity scales with the level of

286   local firing. The ratio of these two bandwidths, therefore, is a measure of the degree to which

287   synaptic volleys induce local postsynaptic firing. The gamma / delta ratio for the wild-type

288   brain slices was significantly larger than recorded in the PGC-1α$^{PV-/-}$ brain slices, when all pre-

289   ictal events were included (Figure 4C,D), and the difference between groups was maintained

290   when the analysis was restricted to the events in the 100s prior to the SLE (Figure 4E,F) (there

291   was a fractional drop in the gamma/delta ratio for the PGC-1α$^{PV-/-}$ brain slices in this final

292   100s).

293   To investigate these differences further, we made paired patch clamp recordings from PV

294   interneurons and pyramidal cells (Figure 5). The pyramidal recording was made in whole cell

295   voltage-clamp mode, to record the synaptic bombardment, while the PV recording was made

296   in cell-attached mode, to record the firing pattern (Figure 5Ai,Bi). This allowed us to compare

297   the level of PV participation in these discharges, in the wild-type and PGC-1α$^{PV-/-}$ experimental

298   groups. We found that PV firing rates were significantly lower in the PGC-1α$^{PV-/-}$ brain slices

299   compared with wild-type brain slices prior to the first SLE (Figure 6Ai), although this

300   difference was not maintained in later interictal events (Figure 6Aii). The number of action

301   potentials per discharge (Figure 6B), and the action potential durations (Figure 6C), were

302   equivalent in the wild-type and PGC-1α$^{PV-/-}$ brain slices.

303   We then repeated the experiment, but instead, recording the firing patterns of the

304   pyramidal cells (Figure 7). The numbers of action potentials per discharge was similar for the

305   two experimental groups (Figure 8A), but the maximal firing rate for the PGC-1α$^{PV-/-}$ brain

306   slices was significantly lower than for the wild-type brain slices, consistent with the lower

307   gamma/delta ratio (Figure 8B). This difference was seen when analyses included all interictal

308   pathological discharges (Figure 8Bii), or if the analysis was restricted just to the events prior

309   to the first SLE (Figure 8Bi). There was no difference in the half-width of the action potentials

310   in the two groups (Figure 8C). These analyses show, therefore, that even though the genetic

311   manipulation was restricted to the PV interneuronal cell class, the network impact was felt

312   more widely across the network.

313

Discussion

315   We have shown in these studies that knocking down the transcriptional coactivator, PGC-

316   1α, specifically in PV interneurons, reduces network excitability. Our focus upon this

317   subpopulation of interneurons was motivated in part because they have been postulated to play

318   pivotal roles in various physiological brain rhythms (Cobb et al., 1995; Sohal et al., 2009;

319   Traub and Miles, 1991), as well as both opposing (Parrish et al., 2019; Trevelyan, 2016), and

320   promoting (Chang et al., 2018), seizure-like activity in different situations (note that these two

321   statements are not necessarily incompatible – see (Burman et al., 2019; Cossart et al., 2005;

322   Ellender et al., 2014; Sessolo et al., 2015)). Finally, there is a close relationship between PGC-

323   1α and PV expression (Lucas et al., 2010), for which we provide further evidence, by showing

324   that activity dependent regulation of genes downstream of PGC-1α such as PV is lost in the

325   knock out (Figure 1 B, C and D). The anti-epileptic effect reflects a reduction in the intensity

326   of pre-ictal bursts, measured both by the high-gamma power, and also by the firing rates of

327   both PV interneurons and pyramidal cells.

328   The effect on PV interneuronal firing could be understood as a direct consequence of the

329   fact that these are the cells in which PGC-1α is knocked-down. As such, it could be interpreted

330   as an adaptation to a mutation which limits energy production, by limiting also the energy

331   expenditure. However, the secondary, effect on pyramidal firing tells us that there are indirect

332   consequences of the cell-specific knock-down, and given that interneuronal firing is driven by

333   pyramidal activity, there are clearly more complex feedback loops that cloud any simple

334   interpretation of the results. This is further complicated by other effects, such as the reduction

335   in expression of genes downstream of PGC-1α; synaptotagmin 2 (Syt2) and complexin 1

336   (Cplx1). Syt2 and Cplx1 are synaptic proteins which act to promote synchronous

337   neurotransmitter release from PV cells and their expression levels are reduced in PGC-1$\alpha^{PV-/-}$

338   mice (Lucas et al., 2014). We confirmed this reduction and additionally showed a lack of

339   activity-dependent regulation of expression levels which resulted in a failure to increase

340   expression in response to induced hyperexcitability.

341   Another interesting element is the reduction also in PV expression in PGC-1$\alpha^{PV-/-}$ mice.

342   PV acts as a slow calcium buffer, helping to protect against hyperexcitability by sequestering

343   away excess Ca^{2+} during periods of intense activity. Altered Ca^{2+} buffering in PGC-1$\alpha^{PV-/-}$ mice

344   may therefore be a factor in the reduced level of interneuronal bursting, although it is notable

345   that the specific knock-down of PV in striatal interneurons is associated with increased

346   excitability (Orduz et al., 2013), the opposite of what we found during induced ictogenesis.

347   The different results may arise for several reasons: our studies involved a reduction in PV

348   expression, rather than a complete PV deficiency; they were of neocortical, rather than striatal

349   interneurons; and the activity patterns and input to PV cells during $0Mg^{2+}$ induced ictogenesis

11

350 may differ substantially from those of electrical stimulation paradigms, and as already

351 mentioned, are influenced by multiple other factors besides.

352 The nonautonomous cellular effect seen in pyramidal cells may also arise through a

353 complex set of interactions. One possibility is suggested by the very rapid escalation of

354 interictal activity intensity in the wild-type experimental group, once it starts (see Figure 4A),

355 relative to that seen in the PGC-1α$^{PV-/-}$ brain slices (Figure 4B). The rate of escalation in

356 epileptiform activity can be explained in terms of the rate of chloride loading, which in turn,

357 depends on the rate of PV firing. Lowering the PV activity, as is seen in the PGC-1α$^{PV-/-}$ brain

358 slices, would reduce this effect, slowing the escalation, and when averaged over multiple

359 preictal events, yields a lower mean discharge rate also for the pyramidal population. In

360 contrast, the intense GABAergic discharges seen in wild-type brain slices, while serving a

361 protective purpose also has the unwanted consequence of loading their postsynaptic target cells

362 with chloride (Thompson and Gahwiler, 1989), thereby contributing to the pathological

363 evolution of activity (Alfonsa et al., 2015; Burman et al., 2019; Cossart et al., 2005; Dzhala et

364 al., 2010; Ellender et al., 2014; Huberfeld et al., 2007; Lillis et al., 2012). This is an example

365 of positive feedback, where raised network activity creates the substrate that facilitates further

366 neuronal activation, that may be critical for seizure initiation (Graham et al., 2021).

367 Early studies of PGC-1α identified its thermogenic role in skeletal muscle and brown fat,

368 by uncoupling mitochondrial respiration in response to cold (Puigserver et al., 1998);

369 interestingly, cold does not induce PGC-1α in the brain. There, its role may relate to protection

370 against other stresses, including cytokines and lipopolysaccharides (McMeekin et al., 2021;

371 Puigserver et al., 2001). For instance, PGC-1α leads to increases in expression of various

372 enzymes involved in detoxification of reactive oxygen species (Austin and St-Pierre, 2012).

373 Conversely, in mouse models of stress, PGC-1α reduction associated with increased markers

374 of oxidative stress, are found within cortical PV interneurons (Jiang et al., 2013b). The cellular

375 mechanism appears to involve activation of the p38 MAPK pathway, leading to

376 phosphorylation of PGC-1α, which stabilizes the protein and increases its transcription

377 inducing activity (Puigserver et al., 2001). It is noteworthy therefore, that inhibition of the p38

378 MAPK pathway has also been reported to increase the latency to the first seizure, following

379 pilocarpine treatment (Zhou et al., 2020). That is to say, the pharmacological blockade of

380 MAPK and the knockdown of one of its targets, PGC-1α, as we show in this study, appear to

381 have similar effects, both slowing the pathological process in acute models of ictogenesis.

382 Inhibiting p38 MAPK also reduces the frequency of seizures, and the level of associated

12

383   pathological damage within the hippocampus (Zhou et al., 2020). In contrast, periods of status

384   epilepticus activate p38 MAPK, and this may mediate the subsequent anatomical changes

385   within the cortical networks (Hu et al., 2020).

386   Reduced PGC-1α has been associated with a range of neurological conditions

387   (Christoforou et al., 2007; Cui et al., 2006; Jiang et al., 2013a; Qin et al., 2009; Sheng et al.,

388   2012; Witte et al., 2013; Zheng et al., 2010), but not, to date, with epilepsy. The most pertinent

389   of these to our study is the association with schizophrenia (Christoforou et al., 2007; Jiang et

390   al., 2013a), for which the pathophysiological role of PGC-1α is also believed to be manifest

391   through the PV interneurons within cortical networks (Bartley et al., 2015; Jiang et al., 2013a).

392   The clinical association between epilepsy and schizophrenia is well established, with the

393   existence of one condition carrying around a 6-8-fold increase in risk for having the other

394   (Chang et al., 2011). Previous work reported that knocking down PGC-1α in PV interneurons

395   alters the asynchronous synaptic release of GABA (Lucas et al., 2014), which may be expected

396   to alter how PV interneurons influence spike timing and information flow through cortical

397   networks. Our work suggests that different forms of PV interneuron pathophysiology, relevant

398   to epilepsy and schizophrenia, are distinguished by the level of involvement of PGC-1α.

399

400

13

401   **Figures**
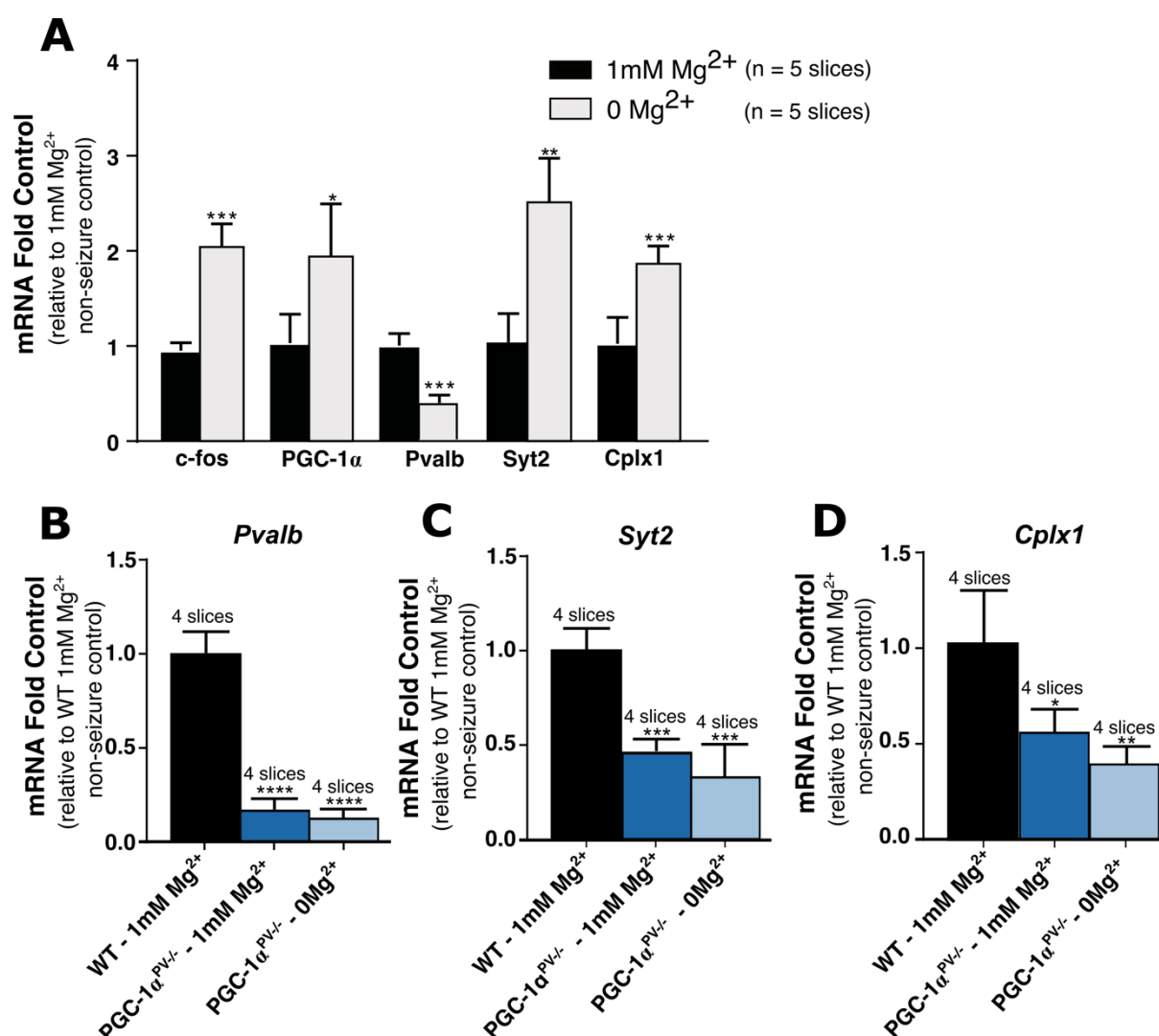
404   **Figure 1. Ictogenesis induced gene-expression changes are markedly altered in PGC-**
405   **1α^{PV-/-} mice.** (A) Shows the increased expression of c-fos, PGC-1α, parvalbumin (Pvalb),
406   synaptotagmin 2 (Syt2) and complexin 1 (Cplx1) after 1 hour being bathed in 0mM Mg^{2+}
407   ACSF, relative to non-seizure control (1mM Mg^{2+}). (**B**-**D**) mRNA levels for parvalbumin
408   (*Pvalb*) (**B**), synaptotagmin 2 (*Syt2*) (**C**) and complexin 1 (*Cplx1*) (**D**), normalised to the mean
409   for wild-type brain slices kept 1hr in normal 1mM Mg^{2+} ACSF ("control", black). The relative
410   change in mRNA is shown also for brain slices, prepared from mice with PGC-1α knocked-
411   out in PV cells, and bathed either in normal 1mM Mg^{2+} (dark blue) or in 0mM Mg^{2+} ACSF
412   (light blue). * $p < 0.05$; ** $p < 0.01$; *** $p < 0.001$; **** $p < 0.0001$.

413
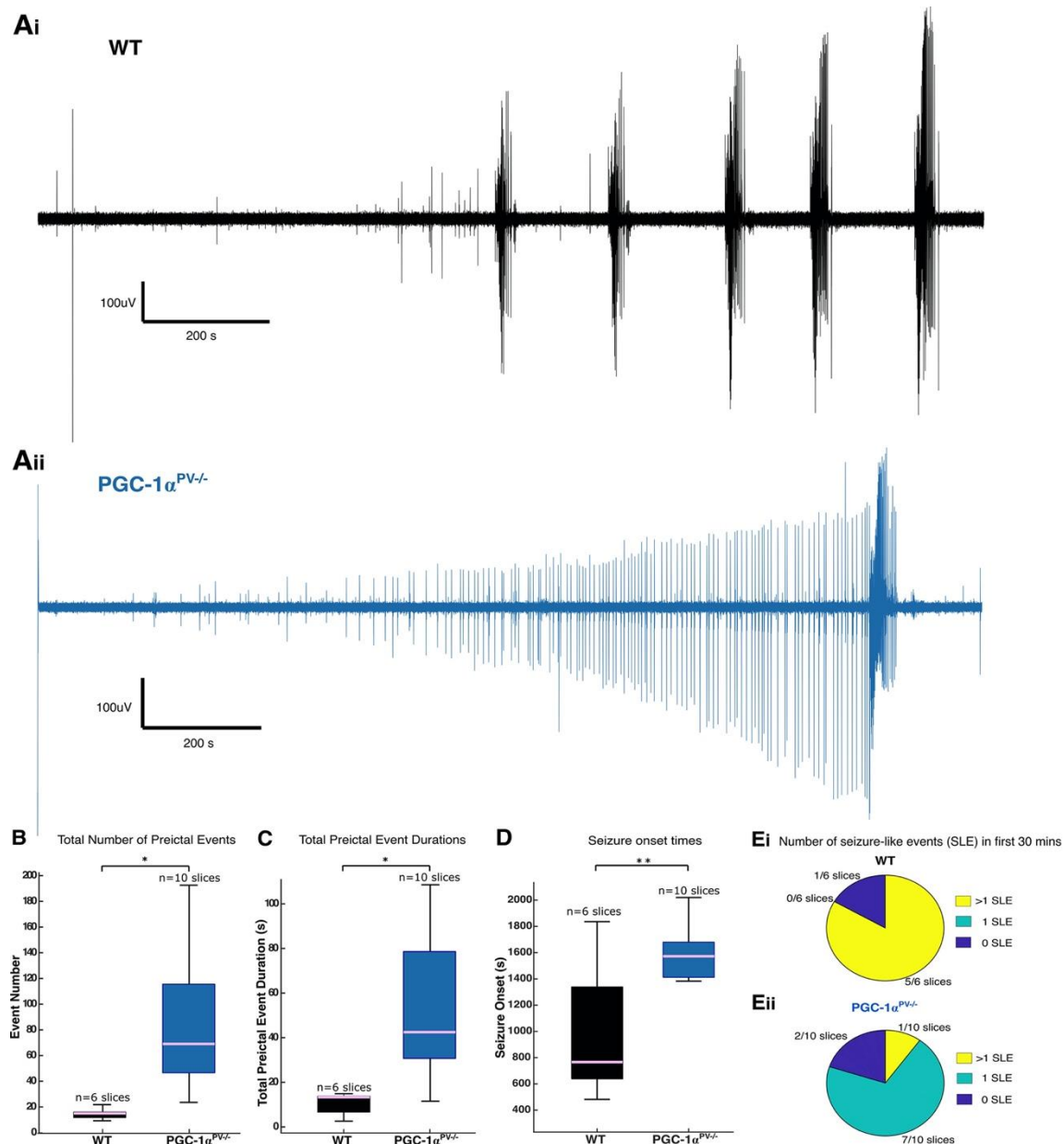
Figure 2. Markedly different patterns of epileptiform activity leading up to the first SLE, in brain slices prepared from PGC-1α and wild-type mice. (A) Representative LFP recordings of neocortical activity during $0Mg^{2+}$-induced ictogenesis in brain slices prepared either from wild-type (Ai) or PGC-1α$^{PV-/-}$ mice (Aii). (B) Boxplot showing the total number of preictal events (events prior to first seizure-like event (SLE; pink line = median; boxed region = interquartile range; whiskers – full data range) for wild-type (black) and PGC-1α$^{PV-/-}$ mice (blue). (C) Boxplot showing the total cumulative duration of pathological preictal activity. (D) Boxplot showing the latency to the first SLE. (E) Pie charts showing the number of SLEs in the first 30 minutes in $0Mg^{2+}$ for wild-type (Ei) and PGC-1α$^{PV-/-}$ mice (Eii). No SLEs (dark blue), one SLE (turquoise) and more than one SLE (yellow). * $p < 0.05$; ** $p < 0.01$.

15
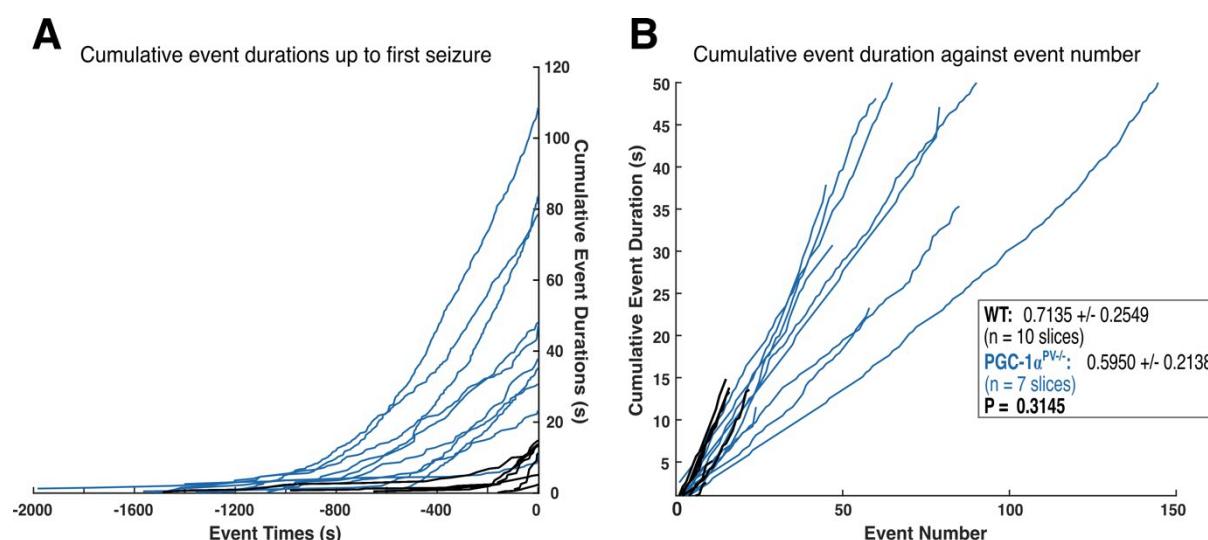
**Figure 3. PGC-1α^PV-/- mice show far greater cumulative pathological activity prior to the onset of SLEs, compared to wild-type mice.** (A) The cumulative total duration of the preictal pathological activity leading up to the onset of the first seizure-like event (SLE, designated t = 0s). (B) Shows the cumulative events durations with progressing event number for wild-type (black) and PGC-1α^PV-/- mice (blue). Note the steady gradients (inset box), indicative that the event durations do not change appreciably over time.

16
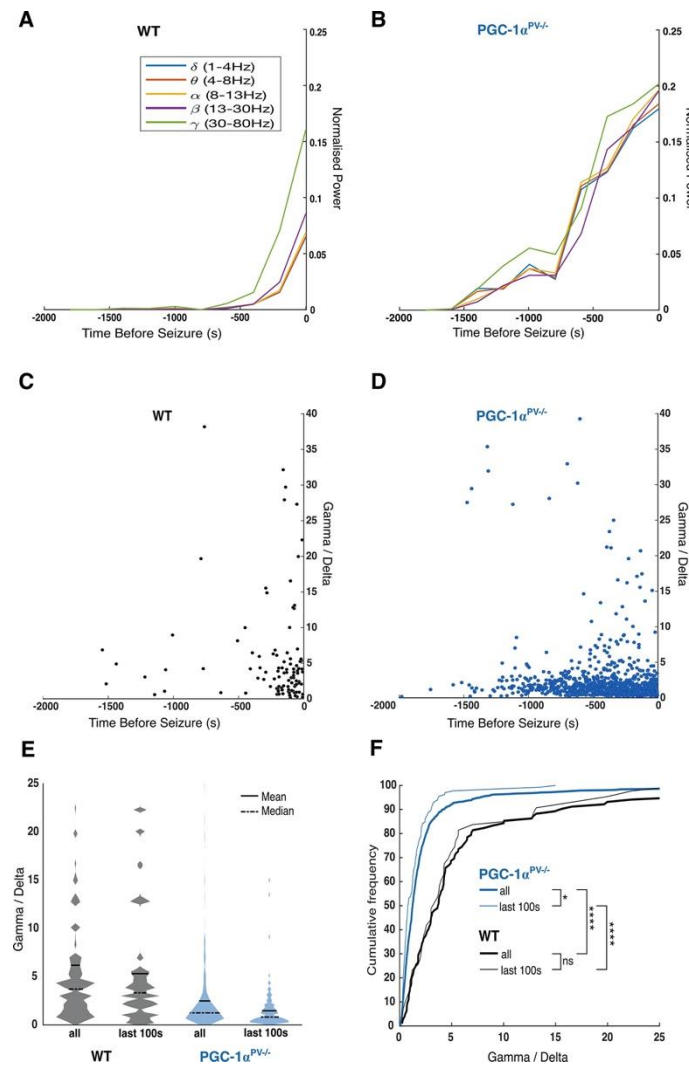
Figure 4. Preictal discharges in brain slices from PGC-1α knock-out mice show reduced normalised gamma activity (γ/δ ratio), compared to wild-type mice. (**A**) The mean normalised power, for the main physiological LFP bandwidths as indicated, averaged for sequential 200s epochs prior to the onset of the first SLE (t = 0s), for wild-type brain slices, recorded in $0 \, Mg^{2+}$ ACSF (n = 7). (**B**) Equivalent data from brain slices from PGC-1α$^{PV-/-}$ mice (n = 10). Note the far more rapid escalation of activity in the wild-type brain slices, especially in the gamma and high-gamma frequency bands, leading up to the first SLE. (**C**) The gamma/delta ratio for every single interictal event, plotted against time relative to the onset of the first SLE, in the wild-type brain slices, and (**D**) in the PGC-1α$^{PV-/-}$ brain slices. (**E**) Violin plots of γ/δ ratios, for the entire data set of interictal events, and also events occurring in the 100s immediately prior to the first SLE. (**F**) Cumulative frequency plots of the same data sets. Note the highly significant difference between WT and knock-out tissue, and the fact that there is minimal, if any, change in the period immediately prior to the SLE. * $p < 0.05$; **** $p < 0.0001$.

17
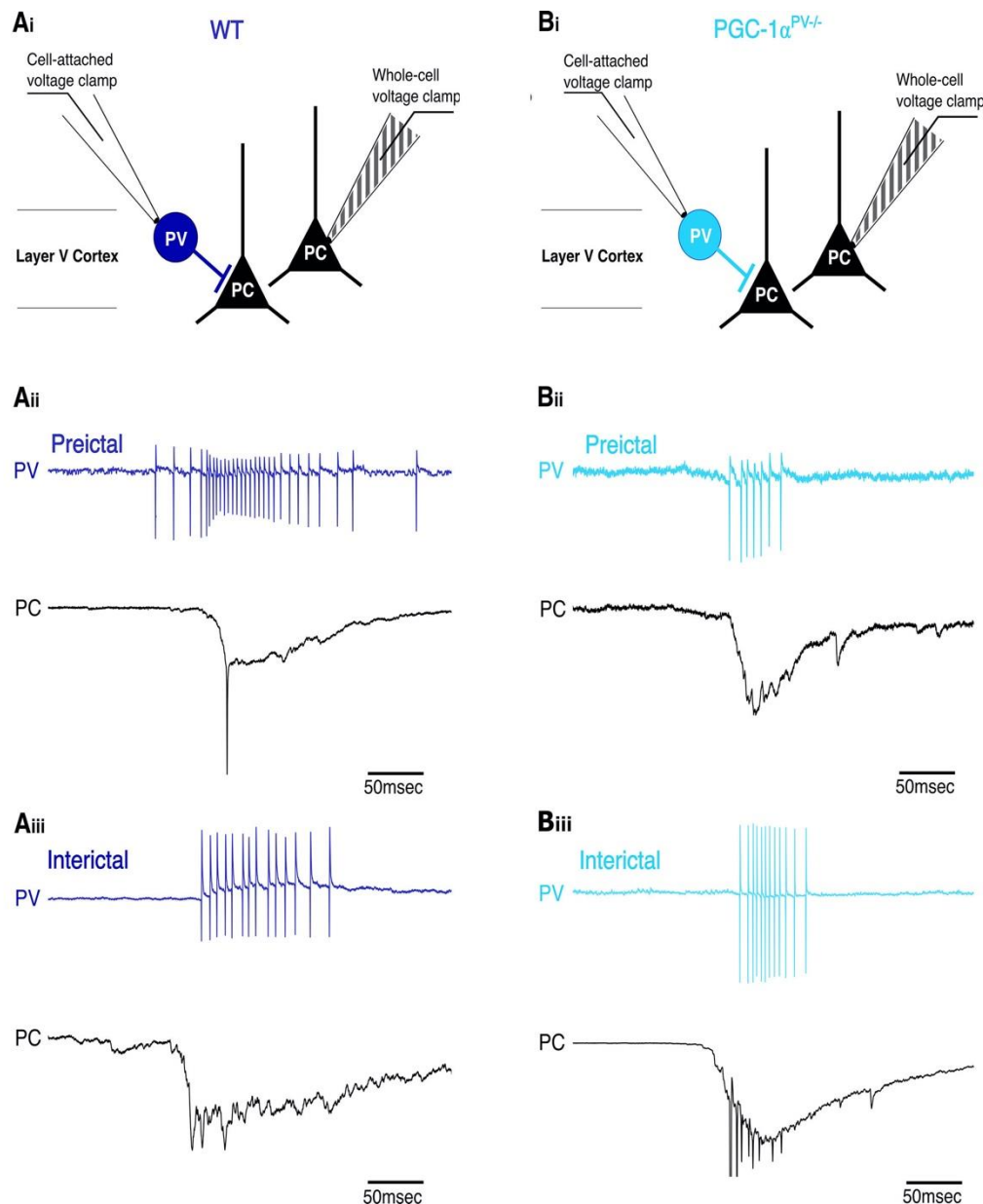
Figure 5. Example PV interneuron preictal and interictal events (**Ai** and **Bi**) The recording configuration for the example traces, below, with a whole-cell, voltage-clamp, pyramidal cell (triangle) recording (shown by the striped electrode) and a cell-attached, voltage-clamp PV interneuron (circle) recording (shown by the clear electrode). The dark red indicates WT and the orange indicates PGC-1α$^{PV-/-}$ mice. The underlying panels show preictal (**Aii**, **Bii**), and interictal (**Aiii**, **Biii**) pyramidal cell and interneuron events. The top traces show the cell-attached recording and the lower traces show the whole-cell recording. WT group, dark blue; PGC-1α$^{PV-/-}$ group, light blue.
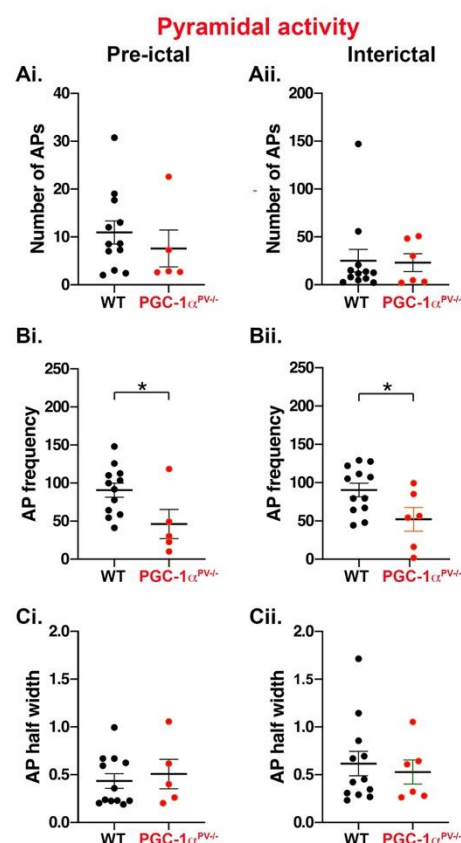
18
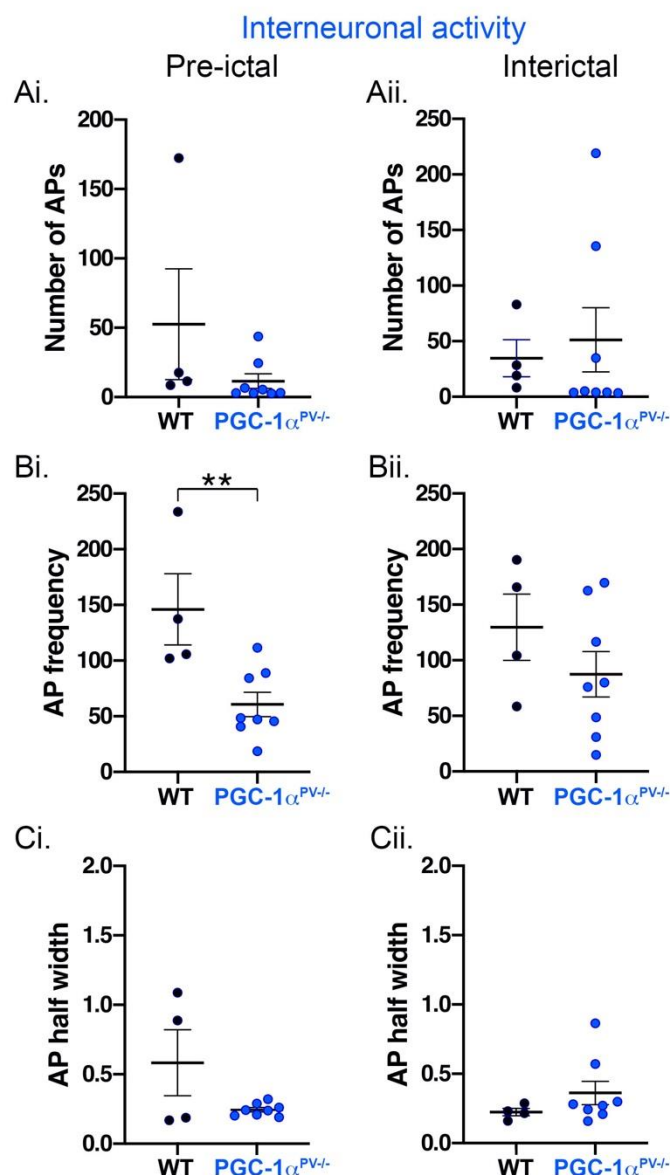
Figure 6. Action potential properties of PV interneurons during preictal and interictal events following 0Mg^{2+}-induced ictogenesis. This figure shows cortical PV interneuron action potential numbers (**Ai**, **Aii**), their frequency (**Bi**, **Bii**) and halfwidths (**Ci**, **Cii**) during preictal (top row) and interictal events (bottom row) induced by 0Mg^{2+}-ictogenic aCSF in control (black) and PGC-1α$^{PV-/-}$ (blue) mouse tissue. Data points show the average data per brain slice. ** $p < 0.01$.

470
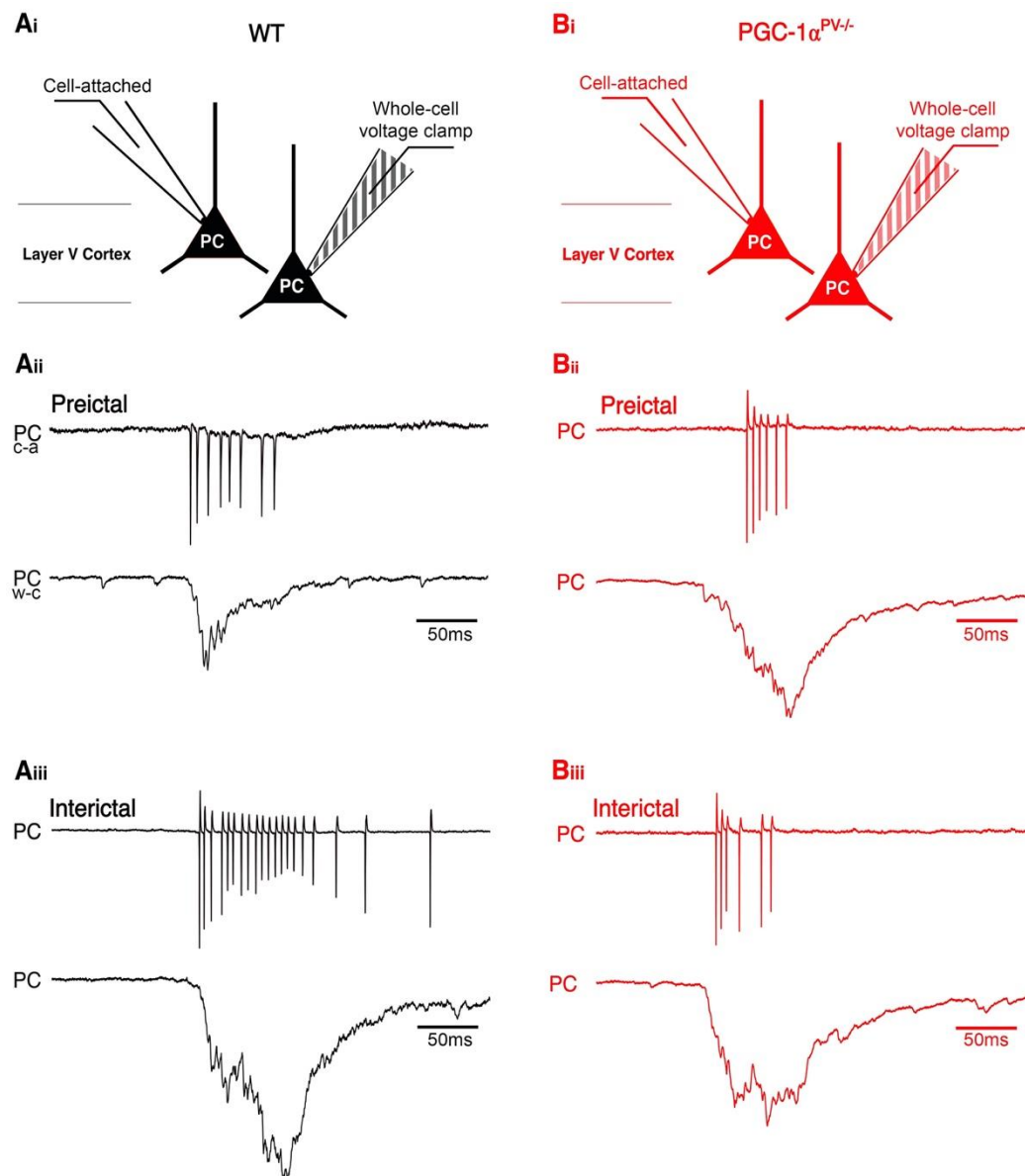
Figure 7. PGC-1α$^{PV-/-}$ mice show reduced pyramidal firing rates, during preictal discharges, compared with wild-type mice. (Ai and Bi) The recording configuration for the underlying traces. The dark blue indicates WT and the light blue indicates PGC-1α$^{PV-/-}$ pyramidal cells. The underlying panels show preictal (Aii, Bii), and interictal (Aiii, Biii) pyramidal cell events. The top traces show the cell-attached recording and the lower traces show the whole-cell recording.

477

478

20

Figure 8. Action potential properties of pyramidal cells during preictal and interictal events following 0Mg²⁺-induced ictogenesis. This figure shows cortical pyramidal cell action potential numbers (**Ai**, **Aii**), their frequency (**Bi**, **Bii**) and halfwidths (**Ci**, **Cii**) during preictal (top row) and interictal events (bottom row) induced by 0Mg²⁺-ictogenic aCSF in control (black) and PGC-1α$^{PV-/-}$ (red) mouse tissue. Data points show the average data per brain slice.

* $p < 0.05$.

References

490

491 Alfonsa, H., Merricks, E.M., Codadu, N.K., Cunningham, M.O., Deisseroth, K., Racca, C., and
492 Trevelyan, A.J. (2015). The contribution of raised intraneuronal chloride to epileptic network
493 activity. J Neurosci *35*, 7715-7726.

494 Atallah, B.V., and Scanziani, M. (2009). Instantaneous modulation of gamma oscillation
495 frequency by balancing excitation with inhibition. Neuron *62*, 566-577.

496 Austin, S., and St-Pierre, J. (2012). PGC1alpha and mitochondrial metabolism--emerging
497 concepts and relevance in ageing and neurodegenerative disorders. J Cell Sci *125*, 4963-4971.

498 Bagattin, A., Hugendubler, L., and Mueller, E. (2010). Transcriptional coactivator PGC-1alpha
499 promotes peroxisomal remodeling and biogenesis. Proc Natl Acad Sci U S A *107*, 20376-
500 20381.

501 Bartley, A.F., Lucas, E.K., Brady, L.J., Li, Q., Hablitz, J.J., Cowell, R.M., and Dobrunz, L.E.
502 (2015). Interneuron Transcriptional Dysregulation Causes Frequency-Dependent Alterations
503 in the Balance of Inhibition and Excitation in Hippocampus. J Neurosci *35*, 15276-15290.

504 Burman, R.J., Selfe, J.S., Lee, J.H., van den Berg, M., Calin, A., Codadu, N.K., Wright, R.,
505 Newey, S.E., Parrish, R.R., Katz, A.A.*, et al.* (2019). Excitatory GABAergic signalling is
506 associated with benzodiazepine resistance in status epilepticus. Brain *142*, 3482-3501.

507 Chang, M., Dian, J.A., Dufour, S., Wang, L., Moradi Chameh, H., Ramani, M., Zhang, L.,
508 Carlen, P.L., Womelsdorf, T., and Valiante, T.A. (2018). Brief activation of GABAergic
509 interneurons initiates the transition to ictal events through post-inhibitory rebound excitation.
510 Neurobiol Dis *109*, 102-116.

511 Chang, Y.T., Chen, P.C., Tsai, I.J., Sung, F.C., Chin, Z.N., Kuo, H.T., Tsai, C.H., and Chou,
512 I.C. (2011). Bidirectional relation between schizophrenia and epilepsy: a population-based
513 retrospective cohort study. Epilepsia *52*, 2036-2042.

514 Christoforou, A., Le Hellard, S., Thomson, P.A., Morris, S.W., Tenesa, A., Pickard, B.S.,
515 Wray, N.R., Muir, W.J., Blackwood, D.H., Porteous, D.J.*, et al.* (2007). Association analysis
516 of the chromosome 4p15-p16 candidate region for bipolar disorder and schizophrenia. Mol
517 Psychiatry *12*, 1011-1025.

518 Cobb, S.R., Buhl, E.H., Halasy, K., Paulsen, O., and Somogyi, P. (1995). Synchronization of
519 neuronal activity in hippocampus by individual GABAergic interneurons. Nature *378*, 75-78.

520 Cossart, R., Bernard, C., and Ben-Ari, Y. (2005). Multiple facets of GABAergic neurons and
521 synapses: multiple fates of GABA signalling in epilepsies. Trends Neurosci *28*, 108-115.

522 Cowell, R.M., Blake, K.R., and Russell, J.W. (2007). Localization of the transcriptional
523 coactivator PGC-1alpha to GABAergic neurons during maturation of the rat brain. J Comp
524 Neurol *502*, 1-18.

525 Cui, L., Jeong, H., Borovecki, F., Parkhurst, C.N., Tanese, N., and Krainc, D. (2006).
526 Transcriptional repression of PGC-1alpha by mutant huntingtin leads to mitochondrial
527 dysfunction and neurodegeneration. Cell *127*, 59-69.

528 Dougherty, S.E., Bartley, A.F., Lucas, E.K., Hablitz, J.J., Dobrunz, L.E., and Cowell, R.M.
529 (2014). Mice lacking the transcriptional coactivator PGC-1alpha exhibit alterations in
530 inhibitory synaptic transmission in the motor cortex. Neuroscience *271*, 137-148.

531 Dragunow, M., and Robertson, H.A. (1987). Kindling stimulation induces c-fos protein(s) in
532 granule cells of the rat dentate gyrus. Nature *329*, 441-442.

22

533 Dzhala, V.I., Kuchibhotla, K.V., Glykys, J.C., Kahle, K.T., Swiercz, W.B., Feng, G., Kuner,
534 T., Augustine, G.J., Bacskai, B.J., and Staley, K.J. (2010). Progressive NKCC1-dependent
535 neuronal chloride accumulation during neonatal seizures. J Neurosci *30*, 11745-11761.

536 Ellender, T.J., Raimondo, J.V., Irkle, A., Lamsa, K.P., and Akerman, C.J. (2014). Excitatory
537 effects of parvalbumin-expressing interneurons maintain hippocampal epileptiform activity via
538 synchronous afterdischarges. J Neurosci *34*, 15208-15222.

539 Graham, R.T., Parrish, R.R., Allberio, L., E.L., J., and Trevelyan, A.J. (2021). Synergistic
540 positive   feedback   underlying   seizure   initiation.   biorXiv
541 *https://doi.org/10.1101/2021.02.28.433224*.

542 Gulyas, A.I., Buzsaki, G., Freund, T.F., and Hirase, H. (2006). Populations of hippocampal
543 inhibitory neurons express different levels of cytochrome c. Eur J Neurosci *23*, 2581-2594.

544 Hajos, N., Palhalmi, J., Mann, E.O., Nemeth, B., Paulsen, O., and Freund, T.F. (2004). Spike
545 timing of distinct types of GABAergic interneuron during hippocampal gamma oscillations in
546 vitro. J Neurosci *24*, 9127-9137.

547 Handschin, C., and Spiegelman, B.M. (2006). Peroxisome proliferator-activated receptor
548 gamma coactivator 1 coactivators, energy homeostasis, and metabolism. Endocr Rev *27*, 728-
549 735.

550 Hu, J.H., Malloy, C., and Hoffman, D.A. (2020). P38 Regulates Kainic Acid-Induced Seizure
551 and Neuronal Firing via Kv4.2 Phosphorylation. Int J Mol Sci *21*.

552 Huberfeld, G., Wittner, L., Clemenceau, S., Baulac, M., Kaila, K., Miles, R., and Rivera, C.
553 (2007). Perturbed chloride homeostasis and GABAergic signaling in human temporal lobe
554 epilepsy. J Neurosci *27*, 9866-9873.

555 Jiang, Z., Cowell, R.M., and Nakazawa, K. (2013a). Convergence of genetic and environmental
556 factors on parvalbumin-positive interneurons in schizophrenia. Front Behav Neurosci *7*, 116.

557 Jiang, Z., Rompala, G.R., Zhang, S., Cowell, R.M., and Nakazawa, K. (2013b). Social isolation
558 exacerbates schizophrenia-like phenotypes via oxidative stress in cortical interneurons. Biol
559 Psychiatry *73*, 1024-1034.

560 Kageyama, G.H., and Wong-Riley, M.T. (1982). Histochemical localization of cytochrome
561 oxidase in the hippocampus: correlation with specific neuronal types and afferent pathways.
562 Neuroscience *7*, 2337-2361.

563 Kann, O. (2016). The interneuron energy hypothesis: Implications for brain disease. Neurobiol
564 Dis *90*, 75-85.

565 Lillis, K.P., Kramer, M.A., Mertz, J., Staley, K.J., and White, J.A. (2012). Pyramidal cells
566 accumulate chloride at seizure onset. Neurobiol Dis *47*, 358-366.

567 Lin, J., Handschin, C., and Spiegelman, B.M. (2005). Metabolic control through the PGC-1
568 family of transcription coactivators. Cell Metab *1*, 361-370.

569 Lin, J., Wu, P.H., Tarr, P.T., Lindenberg, K.S., St-Pierre, J., Zhang, C.Y., Mootha, V.K., Jager,
570 S., Vianna, C.R., Reznick, R.M.*, et al.* (2004). Defects in adaptive energy metabolism with
571 CNS-linked hyperactivity in PGC-1alpha null mice. Cell *119*, 121-135.

572 Lucas, E.K., Dougherty, S.E., McMeekin, L.J., Reid, C.S., Dobrunz, L.E., West, A.B., Hablitz,
573 J.J., and Cowell, R.M. (2014). PGC-1alpha provides a transcriptional framework for
574 synchronous neurotransmitter release from parvalbumin-positive interneurons. J Neurosci *34*,
575 14375-14387.

23

Lucas, E.K., Dougherty, S.E., McMeekin, L.J., Trinh, A.T., Reid, C.S., and Cowell, R.M. (2012). Developmental alterations in motor coordination and medium spiny neuron markers in mice lacking pgc-1alpha. PLoS One *7*, e42878.

Lucas, E.K., Markwardt, S.J., Gupta, S., Meador-Woodruff, J.H., Lin, J.D., Overstreet-Wadiche, L., and Cowell, R.M. (2010). Parvalbumin deficiency and GABAergic dysfunction in mice lacking PGC-1alpha. J Neurosci *30*, 7227-7235.

McMeekin, L.J., Fox, S.N., Boas, S.M., and Cowell, R.M. (2021). Dysregulation of PGC-1alpha-Dependent Transcriptional Programs in Neurological and Developmental Disorders: Therapeutic Challenges and Opportunities. Cells *10*.

Morgan, J.I., Cohen, D.R., Hempstead, J.L., and Curran, T. (1987). Mapping patterns of c-fos expression in the central nervous system after seizure. Science *237*, 192-197.

Orduz, D., Bischop, D.P., Schwaller, B., Schiffmann, S.N., and Gall, D. (2013). Parvalbumin tunes spike-timing and efferent short-term plasticity in striatal fast spiking interneurons. J Physiol *591*, 3215-3232.

Parrish, R.R., Codadu, N.K., Mackenzie-Gray Scott, C., and Trevelyan, A.J. (2019). Feedforward inhibition ahead of ictal wavefronts is provided by both parvalbumin- and somatostatin-expressing interneurons. J Physiol *597*, 2297-2314.

Puigserver, P., Rhee, J., Lin, J., Wu, Z., Yoon, J.C., Zhang, C.Y., Krauss, S., Mootha, V.K., Lowell, B.B., and Spiegelman, B.M. (2001). Cytokine stimulation of energy expenditure through p38 MAP kinase activation of PPARgamma coactivator-1. Mol Cell *8*, 971-982.

Puigserver, P., Wu, Z., Park, C.W., Graves, R., Wright, M., and Spiegelman, B.M. (1998). A cold-inducible coactivator of nuclear receptors linked to adaptive thermogenesis. Cell *92*, 829-839.

Qin, W., Haroutunian, V., Katsel, P., Cardozo, C.P., Ho, L., Buxbaum, J.D., and Pasinetti, G.M. (2009). PGC-1alpha expression decreases in the Alzheimer disease brain as a function of dementia. Arch Neurol *66*, 352-361.

Saunders, A., Macosko, E.Z., Wysoker, A., Goldman, M., Krienen, F.M., de Rivera, H., Bien, E., Baum, M., Bortolin, L., Wang, S.*, et al.* (2018). Molecular Diversity and Specializations among the Cells of the Adult Mouse Brain. Cell *174*, 1015-1030 e1016.

Sessolo, M., Marcon, I., Bovetti, S., Losi, G., Cammarota, M., Ratto, G.M., Fellin, T., and Carmignoto, G. (2015). Parvalbumin-Positive Inhibitory Interneurons Oppose Propagation But Favor Generation of Focal Epileptiform Activity. J Neurosci *35*, 9544-9557.

Sheng, B., Wang, X., Su, B., Lee, H.G., Casadesus, G., Perry, G., and Zhu, X. (2012). Impaired mitochondrial biogenesis contributes to mitochondrial dysfunction in Alzheimer's disease. J Neurochem *120*, 419-429.

Sohal, V.S., Zhang, F., Yizhar, O., and Deisseroth, K. (2009). Parvalbumin neurons and gamma rhythms enhance cortical circuit performance. Nature *459*, 698-702.

St-Pierre, J., Lin, J., Krauss, S., Tarr, P.T., Yang, R., Newgard, C.B., and Spiegelman, B.M. (2003). Bioenergetic analysis of peroxisome proliferator-activated receptor gamma coactivators 1alpha and 1beta (PGC-1alpha and PGC-1beta) in muscle cells. J Biol Chem *278*, 26597-26603.

Thompson, S.M., and Gahwiler, B.H. (1989). Activity-dependent disinhibition. I. Repetitive stimulation reduces IPSP driving force and conductance in the hippocampus in vitro. J Neurophysiol *61*, 501-511.

620 Traub, R.D., and Miles, R. (1991). Neuronal networks of the hippocampus (Cambridge, UK:
621 Cambridge University Press).

622 Trevelyan, A.J. (2016). Do Cortical Circuits Need Protecting from Themselves? Trends
623 Neurosci *39*, 502-511.

624 White, J.D., and Gall, C.M. (1987). Differential regulation of neuropeptide and proto-oncogene
625 mRNA content in the hippocampus following recurrent seizures. Brain Res *427*, 21-29.

626 Whittaker, R.G., Turnbull, D.M., Whittington, M.A., and Cunningham, M.O. (2011). Impaired
627 mitochondrial function abolishes gamma oscillations in the hippocampus through an effect on
628 fast-spiking interneurons. Brain *134*, e180; author reply e181.

629 Whittington, M.A., and Traub, R.D. (2003). Inhibitory interneurons and network oscillations
630 in vitro. Trends Neurosci *26*, 676-682.

631 Witte, M.E., Nijland, P.G., Drexhage, J.A., Gerritsen, W., Geerts, D., van Het Hof, B.,
632 Reijerkerk, A., de Vries, H.E., van der Valk, P., and van Horssen, J. (2013). Reduced
633 expression of PGC-1alpha partly underlies mitochondrial changes and correlates with neuronal
634 loss in multiple sclerosis cortex. Acta Neuropathol *125*, 231-243.

635 Zheng, B., Liao, Z., Locascio, J.J., Lesniak, K.A., Roderick, S.S., Watt, M.L., Eklund, A.C.,
636 Zhang-James, Y., Kim, P.D., Hauser, M.A.*, et al.* (2010). PGC-1alpha, a potential therapeutic
637 target for early intervention in Parkinson's disease. Science translational medicine *2*, 52ra73.

638 Zhou, X., Chen, Q., Huang, H., Zhang, J., Wang, J., Chen, Y., Peng, Y., Zhang, H., Zeng, J.,
639 Feng, Z.*, et al.* (2020). Inhibition of p38 MAPK regulates epileptic severity by decreasing
640 expression levels of A1R and ENT1. Mol Med Rep *22*, 5348-5357.

641

25